Zinc oxide nanoparticles development using phosphorylated alginate template matrix for water treatment applications: I. removal of methylene blue dye

A.M. Omer[a], T.M. Tamer[a], W.M. Abou-Taleb[b], G.D. Roston[c], A.M. Hafez[b], E.F. Shehata[b], R.E. Khalifa[a], M.S. Mohyeldin[a,*]

[a]*Polymer Materials Research Department, Advanced Technology and New Materials Research Institute (ATNMRI),*
City of Scientific Research and Technological Applications (SRTA-City), New Borg El-Arab City, 21934, Alexandria, Egypt,
emails: mohyeldinmohamed@gmail.com (M.S. Mohyeldin), ahmedomer_81@yahoo.com (A.M. Omer), ttamer85@yahoo.com (T.M. Tamer),
randaghonim@yahoo.com (R.E. Khalifa)
[b]*Physical Department, Faculty of Education, Alexandria University, Alexandria, Egypt, emails: wmaboutaleb@gmail.com (W.M. Abou-Taleb),*
ahmmed_hafez@yahoo.com (A.M. Hafez), eslam_fadl@yahoo.com (E.F. Shehata)
[c]*Physics Department, Faculty of Science, Alexandria University, Alexandria, Egypt, email: Dr.gamal_daniel@yahoo.com*

ABSTRACT

In the current work, a highly chelating alginate derivative (phosphorylated alginate [PhAlg]) used as a template for the development of zinc oxide (ZnO) nanoparticles for the first time. Zn^{2+} ions were employed for gelation of the phosphorylated alginate, and then the ZnO nanoparticles were formed via annealing of (Zn-PhAlg) hydrogel. Different particles sizes of the ZnO nanoparticles were obtained by variation of the used PhAlg solution concentration. Properties of the obtained ZnO nanoparticles were verified using characterization tools such as FT-IR, SEM, and surface area measurements. Batch experiments were used to study the ability of the prepared zinc oxide nanoparticles for removing methylene blue (MB) from its aqueous solutions under different operational conditions such as initial MB concentration, pH, adsorbent dosage, contact time and temperature. The results further fitted with different kinetic and isotherm models. Moreover, the thermodynamics of the adsorption process was investigated.

Keywords: Zinc oxide; Nanoparticles; Polymer template; Phosphonate alginate; Dye removal; Kinetics; Isotherm; Thermodynamics

1. Introduction

Nanoparticles present new or enhanced features which established with specific characteristics such as size, morphology, and distribution. There are dramatic developments in the field of nanotechnology within the recent past years, with numerous developed methodologies to prepare nanoparticles with specific design and size which were counted for specific needs. New applications of nanomaterials and nanoparticles are developing rapidly, such as water treatment, antibacterial, medical and pharmaceutical applications, etc. [1,2].

Zinc oxide nanostructures have caught extensive attention due to their remarkable performance in electronics, optics, and photonics. Several strategies have been utilized to produce ZnO nanoparticles such as sol-gel, microemulsion

* Corresponding author.

techniques, spray pyrolysis, laser ablation, thermal evaporation, chemical deposition, microwave method, mechanical milling and hydrothermal synthesis [3–13]. The main developed synthetic routes of oxide materials with a particular emphasis on the gel-template ones using alginate as an efficient raw material were reviewed [14]. A brief review of the recent advances in metal oxide preparation by the mineralization process of biopolymers, including alginate, shows the diversity of the approaches, and their adaptations to produce materials with potential applications in catalysis, energy and environment preservation sectors [15].

The shape and the size of the metal oxides nanomaterials developed could be controlled by selection of the polymer template and the preparation conditions [16–23]. Mixed metal oxides have applications as adsorbents in organic reactions [16]. Diblock copolymer matrix was used as a template and produced ZnO nanoparticles having a size ranging from 7 to 15 nm [17]. Selection of the alginate salt succeeds in the developing of nanowires or nanoparticles metal oxide [18]. Nano zinc oxide (ZnO) with moderate surface area and high pore volume has been produced using chitosan template [19]. Rice as a bio-template used to modify the shape and size of zinc oxide particles. Pore size and texture of the resulting zinc oxide particles were found to be template-dependent [20]. The average crystallite sizes of the nanoparticles obtained using cellulose and alginate templates were well below 50 nm [21] and in the range of 21–24 nm using starch as template [22]. Further reduction of the ZnO nanospheres size, reaching to average 5 nm, was obtained using sodium alginate as a template [23].

In recent years, there is an increase in the generation of hazardous organic pollutant materials in wastewater [24,25] that drive the scientists to find more efficient treatments designed to reduce pollutant concentration; such as flocculation, ozonation and adsorption [26]. The dyes are extensively used in textile, printing, cosmetics, food processing etc.; in recent years, environmental pollution caused by the release of toxic chemicals from industries. The toxic effluents cause various environmental and health hazards [27]. Methylene blue (MB) is one of the famous dyes used in the industrial dying processes. Removal of MB from dyes wastewater has attracted much attention in the last decade. Among different adsorbent materials used in the MB removal process, ZnO has a significant contribution [28–32].

In this study, zinc oxide nanoparticles with varied size were prepared using phosphonate alginate as a polymeric template for Zn^{2+} ions. The obtained ZnO nanoparticles were evaluated as MB cationic dye absorbent materials. The adsorption data fitted with kinetic, isothermal and thermodynamic models.

2. Materials and methods

2.1. Materials

Zinc acetate dehydrates Zn $(O_2CCH_3)_2$ $(H_2O)_2$ were purchased from Sigma-Aldrich, Sodium alginate $(C_6H_7O_6Na)$ medium viscosity purchased from Alpha chemika, India. Epichlorohydrin (purity 99.5%) supplied by Sigma-Aldrich Chemie Gmbh (USA). Orthophosphoric acid (purity 85% extra pure) supplied by Sigma-Aldrich Chemicals Ltd. (Germany).

2.2. Methods

2.2.1. Preparation of zinc oxide nanoparticles using phosphorylated alginate as the template

Phosphorylated alginate (Ph Alg) was prepared according to the previously published results [33]. The Ph Alg solution (2.0%) was mixed with zinc acetate solutions (2.0%) using homogenizer to obtain a homogeneous mixture, followed by filtration. The obtained hydrogel was washed with distilled water several times to remove excess zinc acetate. After that, the zinc-Ph Alg hydrogel was dried in the oven at 60°C overnight to remove any moisture. Finally, the dried gel was calcinated in the oven at 700°C for 3.0 h to obtain the final product of nanoscale zinc oxide.

2.2.2. An adsorption experiment: batch equilibrium studies

The stock solution of 1 g/L of Methylene blue dye (1,000 ppm) was prepared by dissolving the appropriate amount of dye in distilled water then the used concentrations were obtained by dilution. All the adsorption experiments conducted in 100 mL flasks by adding a given amount of adsorbent to 25 mL dye solution of different dye concentrations with different pH values and shaking in an orbital shaker for a given time. The adsorbate concentrations in the initial and final aqueous solutions were measured by using UV-Vis spectrophotometer at 664 nm. The amount of dye adsorbed was calculated from the difference between the initial concentration and the equilibrium one. The dye removing percentage was calculated using the following relationships:

$$\text{Dye removing}\% = \frac{(C_0 - C_e)}{C_0} \times 100\% \tag{1}$$

where C_0 is the beginning dye concentration, and C_e is the final dye concentration in supernatant.

The removal capacity is calculated according to the following formula:

$$q\left(\frac{\text{mg}}{\text{g}}\right) = V\frac{(C_0 - C_t)}{M} \tag{2}$$

where q is the uptake capacity (mg/g); V is the volume of MB solution (mL), and M is the mass of ZnO (g).

2.3. Instrumental characterization

2.3.1. Infrared spectroscopic analysis (FT-IR)

The structures of zinc oxide nanoparticles were investigated by carrying FT-IR spectroscopic studies using Fourier transform infrared spectrophotometer (Shimadzu FTIR - 8400 S, Japan).

2.3.2. Scanning electron microscope

0.05 g, of powder, was dispersed in 10 mL ethanol then 100 μL of the solution was spread on a glass slide and allowed to dry. The sample was coated with gold using vacuum

sputter coater. Scanning of coated zinc oxide nanoparticles was carried out using a scanning electron microscope (Jeol Jsm 6360LA, Japan).

2.3.3. Thermal gravimetric analysis

Thermal gravimetric analysis (TGA) of zinc oxide nanoparticles was carried out using a thermogravimetric analyzer (Shimadzu TGA-50, Japan) in temperatures ranging from 25°C to 800°C under nitrogen atmosphere at a gas flow rate of 20 mL/min and a heating rate of 10°C/min.

2.3.4. Particle size analysis

0.1 g of zinc oxide nanoparticles were dispersed in 10 mL of distilled water. Each sample was sonicated using an ultrasonic water bath for 15 min before measured in submicron particle size analyzer (Beckman Coulter N5, USA).

3. Results and discussion

Presence of the carboxylic and the phosphonic groups along the alginate backbone simplified chelating of the Fe^{2+} ions in the polymer network [34]. In the previous work, Zn^{2+} chelated with the carboxylic groups of alginate simultaneously during its gel formation [35]. In the current work, Zn^{2+} will chelate with the carboxylic and the phosphonic groups of phosphorylated alginate simultaneously during its gel formation for the first time. The novelty of the current work comes from the presence of multi chelating groups creating different gelation rate and three network structure and consequently control the particle size of the metal oxide and its surface structure. The produced hydrogel annealed at 700°C in the presence of oxygen air to depredate the polymeric network and to form the ZnO nanoparticles. The prepared zinc oxide nanoparticles were characterized using physico-chemical characterization tools; FT-IR, SEM and particle size analysis. Finally, the prepared ZnO nanoparticles were evaluated in the adsorption process of the MB cationic dye. Factors affecting the adsorption process, such as MB concentration, adsorption time, temperature and pH, have been studied. Besides, the effect of variation of the adsorbent amount and the agitation speed was investigated. The fitting of the adsorption data with different kinetic and isotherm models has been determined. Moreover, the thermodynamic parameters have been calculated. Finally, the effect of varying the ZnO particles size on the adsorption capacity and the distribution coefficient (K_d) of the MB has been evaluated.

3.1. Characterization

3.1.1. Particle size measurement

Table 1 demonstrates the effect of variation of the phosphorylated alginate concentration on the particle size of the obtained zinc oxide. Increasing of the polymer solution concentration induced a decrease of the particle size formed that could be explained by the presence of an excess of the chelating groups vs. Zn^{2+}, which make the homogenous spreading of the Zn^{2+} inside the gels before annealing.

Table 1
Effect of the Ph-alginate concentration on the zinc oxide nanoparticles size (Zn^{+2} solution 2%, 180 min calcinations time, and 700°C calcination temperature)

Ph-alginate concentration (%)	Particle size (nm)
0.5%	193.5
1.0%	174.4
1.5%	164.8
2.0%	138.8
3.0%	98.5

The same behaviour was obtained in previous work using unmodified alginate [35]. The modification of the alginate with phosphate groups, compared with the alginate, reduced the particles size of the formed ZnO particles from 183 to 139 nm under the same preparation conditions; polymer template 2%, zinc acetate 2%, calcination time 180 min and calcination temperature 700°C.

3.1.2. Fourier transforms infrared spectroscopy (FTIR)

The FTIR spectra of ZnO nanoparticles are shown in Fig. 1 where the Zn–O bond appears at around 450–490 cm^{-1} [36]. The bands at approximately 636 and 1,076 cm^{-1} may be related to the formation of zinc phosphate which has corresponding characteristic bands at 635 and 1,066 cm^{-1} [37]. The broad peaks around 3,433 cm^{-1} specified to the O–H stretching mode of hydroxyl group [38,39] and 1,624 cm^{-1} (bending) refers to an asymmetrical stretching band of the zinc carboxylate that may be attributed to carbonate that probably gets from the atmospheric carbon dioxide [40].

3.1.3. Thermal gravimetric analysis

Fig. 2 exhibit thermal gravimetric analyses of zinc oxide nanoparticles fabricated using Ph Alg 2% as a template using 2% of zinc acetate as a source of Zn ions calcinated at 700°C, 3 h. The figure confirming that there is no degradation peak recognized over testing temperature, which proves the thermal stability of the prepared nanoparticles and the complete formation of ZnO nanoparticles.

3.1.4. Scanning electron microscope

Fig. 3 presents SEM images of the prepared zinc oxide nanoparticles developed under the same conditions, 2% zinc acetate, calcination for 3 h at 700°C and 800°C, using 2% phosphorylated alginate and 2% alginate. The morphological structure demonstrates a clear change from nano-rod with terminal pyramids-like particles produced from alginate template to nano-hexagonal crystals produced from phosphorylated alginate template. It was recognized a small salience along with particles surface results of the presence of multi chelating groups along with template polymer (i.e., carboxylic and phosphonic groups). Also, the figure shows that the particles are of crystal shape with growing limitation in the z-direction.
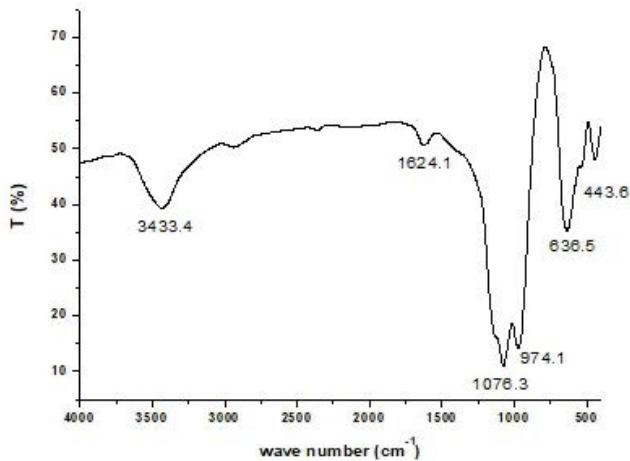
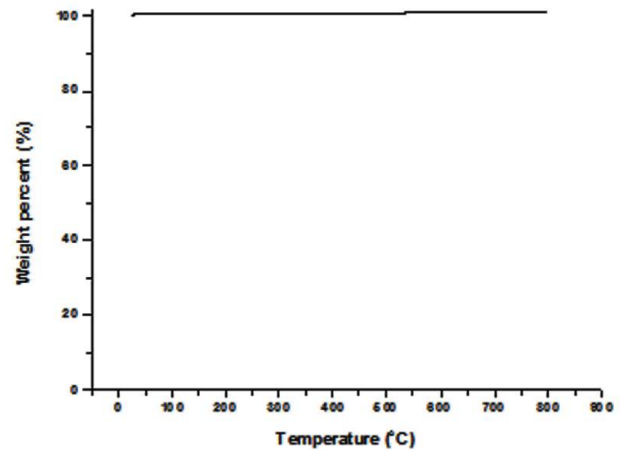Fig. 1. FTIR spectra of the zinc oxide nanoparticles.

Fig. 2. TGA thermograph of the zinc oxide nanoparticles.

Phosphonated alginate template

Phosphonated alginate template
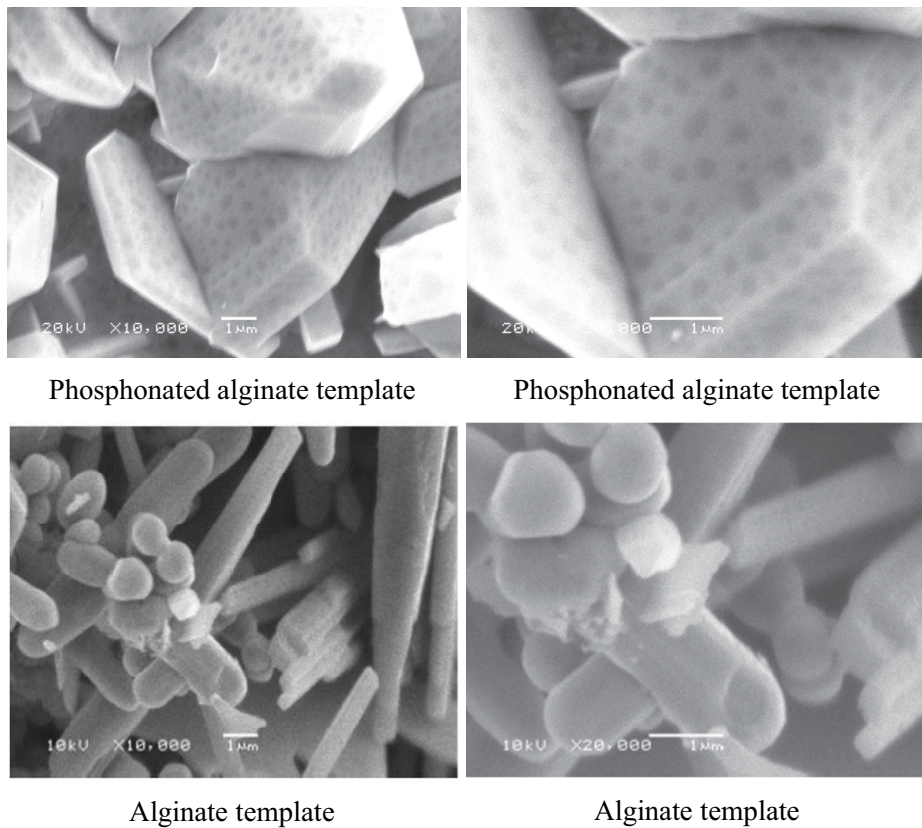
Alginate template

Alginate template

Fig. 3. SEM images of zinc oxide nanoparticles prepared using alginate and phosphonated alginate templates.

3.2. MB adsorption studies onto zinc oxide nanoparticles

In general, zinc oxide and more specific nanoparticles were attracted to the attention of scientists to use for dye removal in wastewater. In the current study, prepared zinc oxide nanoparticles were examined as adsorbents for the dye removal taking methylene blue as a model of a cationic dye. Several factors, such as contact time, solution pH, temperature, MB concentration, adsorbent dosage and ZnO particles size, were studied to explore the adsorption process.

Moreover, the adsorption data were fitted using different kinetic, isothermal and thermodynamic models.

3.2.1. Effect of the adsorption's pH

The pH of the dye solution plays a significant role in the adsorption process. The dye adsorption process is highly pH-dependent, especially for the cationic dye adsorption [41]. It affects the ionization of the adsorptive molecule and therefore, the surface charge of the adsorbent. The attachment

of cationic dyes onto the adsorbent surface is primarily influenced by electrostatic interaction with the adsorbent surface charge, which changed by the pH of the solution. Consequently, studying the effect of pH on the adsorption process is essential in adsorption analyses. In this particular case, the solution pH can change the surface charge of the adsorbent as well as different ionic forms of methylene blue.

Fig. 4 displays the effect of the MB solution pH on its adsorption onto zinc oxide nanoparticles. The maximum adsorption capacity was observed at pH = 7. The adsorption capacity was found minimum at extremely acidic and alkaline MB solutions. A gradual increase was observed from pH 3 (to reach maximum at neutral pH 7), then declined at alkaline pH 9 and 11. At acidic pH, the lower dye sorption may be due to the presence of excess H+ ions struggling with the positive groups on the dye. As the solution pH increased, the active surface sites of ZnO are deprotonated, and the conflict between dye cationic and H+ for the adsorption sites lessens, which decrease the dye decolourization. On the other hand, the higher dye uptake values obtained by increased pH (above pH 3) are due to the electrostatic attraction between the positively charged dyes anions and the immobilized negatively charged ZnO [42].

3.2.2. Effect of the adsorption's temperature

The temperature is also one of the critical factors which influence the adsorption of methylene blue onto nano sorbent. It can change several characters of the adsorption process, for example, the dye solubility, the swelling capacity of the adsorbent, and the equilibrium position concerning the endo- or exothermicity of the adsorption phenomenon [43]. So, the effect of temperature on the stability of MB adsorption onto the synthesized ZnO investigated in the temperature range of 25°C–50°C.

Fig. 5 displays a linear increment of the adsorption capacity by raising temperature in the studied range from 25°C to 50°C. This phenomenon can be explained by increasing the kinetic energy of the MB ions at a higher temperature,
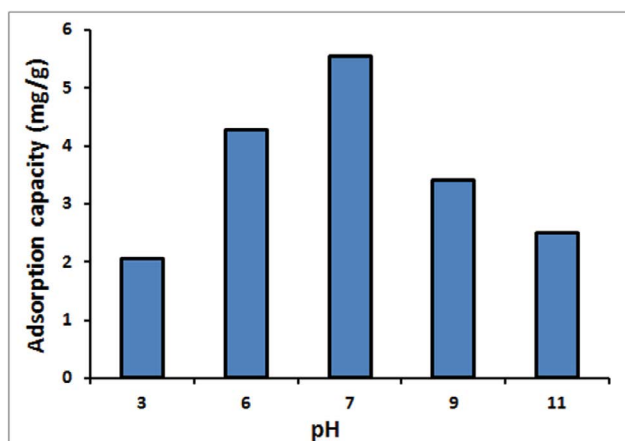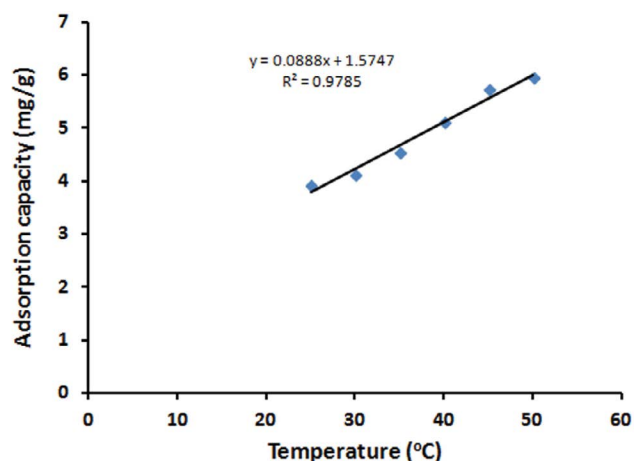

Fig. 5. Effect of the methylene blue solution's temperature on the adsorption capacity of the zinc oxide nanoparticles.

leading to increase in the collision of the MB ions and the ZnO particles [44].

3.2.3. Effect of the adsorbent dosage

Impact of the adsorbent dosage on the adsorption of the methylene blue was studied and recorded at a different portion of nanoparticles ranged from 0.025 to 0.3 g and is presented in Fig. 6. It was seen a decline, almost linear, with an increase of the amount of zinc oxide nanoparticles. This behaviour may be due to the availability of active adsorption sites which dye can get attached to it [45].

3.2.4. Effect of the agitation speed

The result of agitation speed on the adsorption capacity of the ZnO nanoparticles was studied by varying the speed of agitation from 100, 150, 200, 250 to 300 rpm. It can be seen from Fig. 7 that the adsorption capacity almost doubled with an increase of the agitation speed from 100 to 200 rpm. Further improvement of the agitation speed over 200 rpm, the adsorption capacity remained almost constant. These results can be associated with the fact that the increase of the agitation speed, improves the diffusion of MB towards the surface of the adsorbent. That also indicates that a shaking rate of 200 rpm is sufficient to ensure that all primary active sites on the surface are made readily possible for the methylene blue uptake.

3.2.5. Effect of the initial methylene blue concentration

The impact of the initial methylene blue concentration on the adsorption capacity was examined at five different levels of 5, 10, 20, 50, 70 and 100 ppm, and the results are presented in Fig. 8. The adsorption capacity increased linearly with increase in the MB concentration from 5 to 100 ppm. This observation is an indication of the availability of a high number of the free adsorption sites on the surface of the ZnO adsorbent, which directly gave an insight into the adsorption capacity. The great surface area plays a significant role in shifting the equilibrium of the MB molecules

Fig. 4. Effect of the methylene blue solution's pH on the adsorption capacity of the zinc oxide nanoparticles.
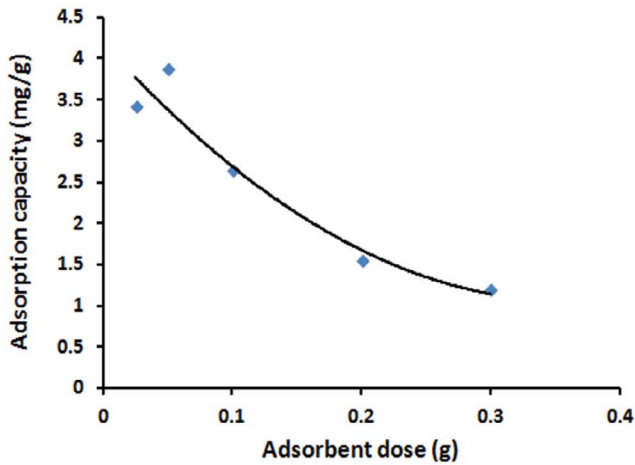
Fig. 6. Effect of the adsorbent dose on its adsorption capacity of MB dye.
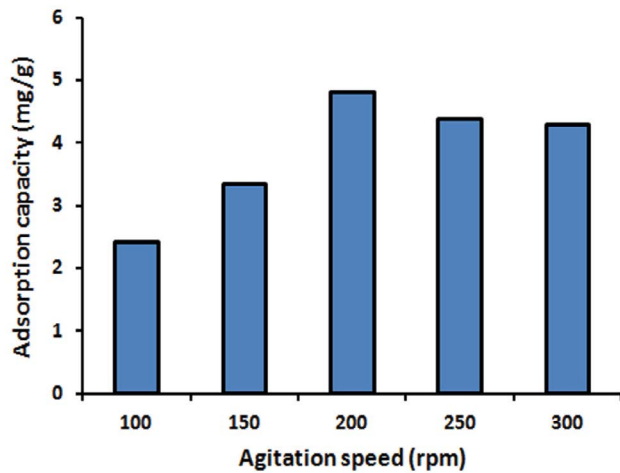

Fig. 7. Effect of the agitation speed on the adsorption capacity of the zinc oxide nanoparticles.
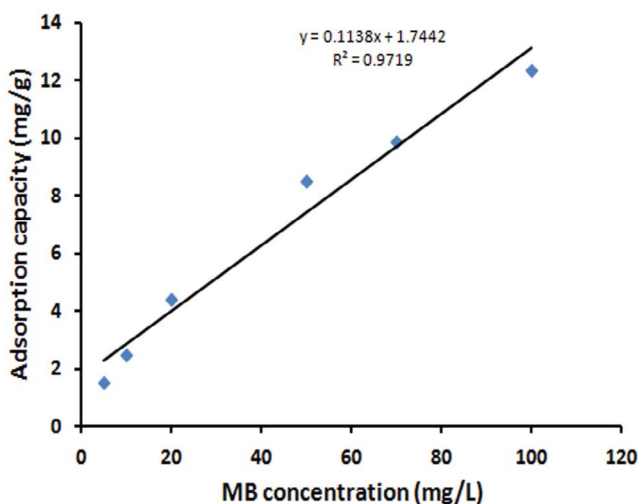

Fig. 8. Effect of the methylene blue concentration on the adsorption capacity of the zinc oxide nanoparticles.

between the solid phase (adsorbent) and the liquid phase (MB solution) to higher concentrations.

3.2.6. Effect of adsorption time

The result of the adsorption time of MB dye onto the zinc oxide nanoparticles was studied over 180 min (Fig. 9). It can be seen from Fig. 9 that the adsorption capacity of the ZnO rapidly increased at the initial period of contact time to 90 min and then approached a slow rate of adsorption capacity at which no more dye was removed from the solution. At this point, the amount of dye adsorbed onto the adsorbent was in a state of dynamic equilibrium with the amount of dye desorbed from the adsorbent. The time required to attain this state of equilibrium termed the equilibrium time, and the amount of dye adsorbed at the equilibrium time reflected the maximum dye adsorption capacity of the adsorbent under these particular conditions.

3.3. Adsorption isotherm models

Adsorption isotherms are mathematical models that describe the distribution of the adsorbate species among solid and liquid phases and are thus crucial from the chemical design point of view. The results obtained on the adsorption of MB onto the ZnO nanoparticles were analyzed by the well-known models given by Freundlich, Langmuir, Temkin and Harkins–Jura. The sorption data obtained for equilibrium conditions have been analyzed by using the linear forms of these kinds of isotherms (Fig. 10).

The Freundlich isotherm presented by Eq. (3) assumes neither homogeneous site energies nor limited levels of sorption [46–48].

$$\ln q_e = \ln K_F + \frac{1}{n_f}\ln C_e \tag{3}$$

The Langmuir isotherm presented by Eq. (4) assumes monolayer sorption onto a completely homogeneous surface with a finite number of identical sites and with negligible
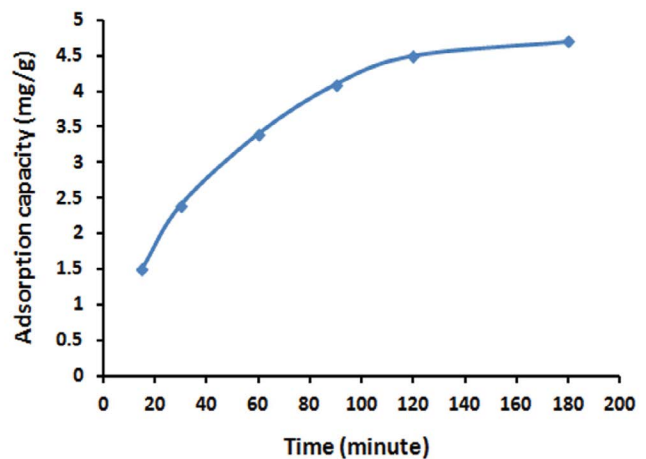

Fig. 9. Effect of the adsorption time on the adsorption capacity of the zinc oxide nanoparticles.
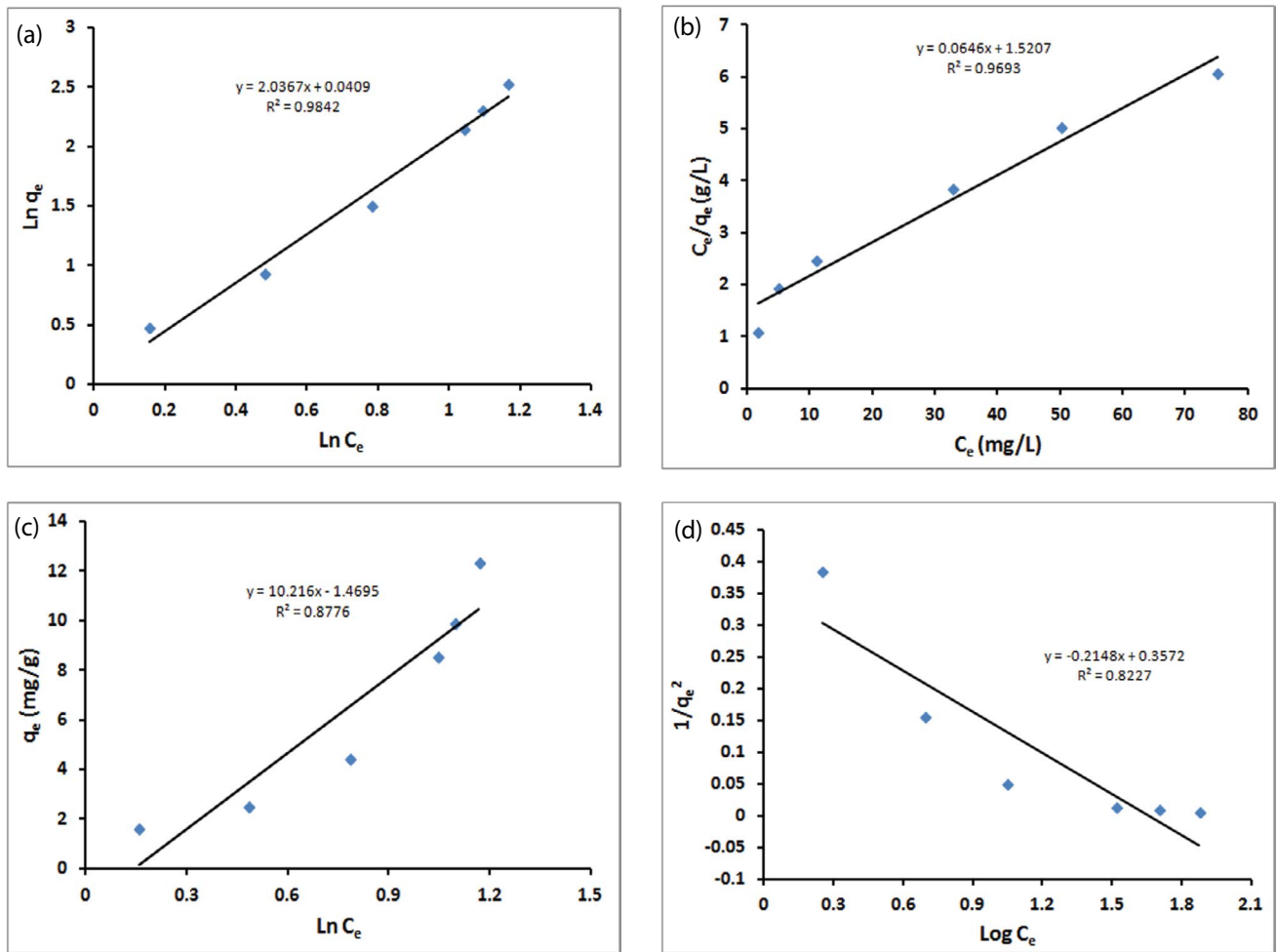
Fig. 10. Adsorption isotherm models: (a) Freundlich, (b) Langmuir, (c) Temkin and (d) Harkins–Jura.

interaction between adsorbed molecules is given by Eq. (4) [49]:

$$\frac{C_e}{q_e} - \frac{1}{q_m K} + \frac{C_e}{q_m} \tag{4}$$

The value R_L calculated (Table 2) according to Eq. (5) [50] fall between zero and one confirmed that the adsorption of the MB onto the ZnO nanoparticles under the conditions used in this study was favourable by Langmuir isotherm [51].

$$R_L = \frac{1}{1 + KC_0} \tag{5}$$

Temkin isotherm considered the effects of indirect adsorbent/adsorbate interactions on the adsorption process [52]. It can be expressed in the linear form as [53,54]:

$$q_e = B\ln K_T + B\ln C_e \tag{6}$$

Finally, the Harkins–Jura adsorption isotherm can be expressed as [55,56].

Table 2
R_L values for different initial MB concentrations

C_0	R_L
5	0.00843
10	0.00423
20	0.00212
50	0.00085
70	0.0006
100	0.00043

$$\frac{1}{q_e^2} = \left(\frac{B_H}{A_H}\right) - \left(\frac{1}{A_H}\right)\log C_e \tag{7}$$

The Harkins–Jura adsorption isotherm accounts to multilayer adsorption and can explain with the existence of heterogeneous pore distribution.

All the isothermal parameter values obtained from the four equilibrium isotherm models applied for the MB adsorption on the ZnO nanoparticles were summarized

in Table 3. Although the Freundlich isotherm model gave the highest R^2 value (0.9842) suggested that the formation of multilayers of adsorption [54,55], the adsorption capacity K_F value, 1.042 mg/g, is far from the experimental value and the $n_f < 1$ indicating unfavourable adsorption for MB using ZnO nanoparticles [56–57]. On the hand, the R^2 value was 0.9693 for Langmuir model is considered an indicator of the goodness-of-fit of experimental data and the maximum adsorption capacity q_{max} closely related from the experimental values which in turn indicated monolayer adsorption of MB onto the ZnO nanoparticles of complete homogeneous surface with a finite number of identical sites and with negligible interaction between MB molecules. The data fitness (R^2) using Temkin and Harkins–Jura adsorption isotherms is lower than both Freundlich and Langmuir isotherms. The Harkins–Jura model shows the smallest fit of the results where R^2 value is 0.8227. The obtained result confirmed the existence of homogeneous pore distribution.

3.4. Adsorption kinetic models

The most common models used to fit the kinetic sorption experiments are Lagergren's pseudo-first-order model (Eq. (8)) [52], pseudo-second-order model (Eq. (9)) [53], and Elovich model (Eq. (10)) [58].

$$\ln\left(q_e - q_t\right) = \ln q_e - K_1 t \tag{8}$$

$$\frac{t}{q_t} = \frac{1}{K_2 q_e^2} + \frac{t}{q_e} \tag{9}$$

$$q_t = \alpha + \beta \ln t \tag{10}$$

where q_e (mg/g) and q_t (mg/g) are the amount of dye adsorbed at equilibrium and at time t, respectively. k_1 (min^{-1}) and k_2 (g mg^{-1} min) are the pseudo-first-order and pseudo-second-order adsorption rate constants, respectively. The Elovich constants are α (mg/g min), the initial sorption rate, and β (g/mg) is the extent of surface coverage and activation energy for chemisorption.

3.4.1. Pseudo-first-order model

The value of the pseudo-first-order constant (k_1; 0.0257) and correlation coefficient (R^2; 0.9817) was obtained from Fig. 11a. It indicated that the correlation coefficients are good enough. However, the estimated value of q_e was calculated from Eq. (8); 5.17 mg/g have differed from the experimental value, 4.7 mg/g.

3.4.2. Pseudo-second-order model

The second-order rate constant (k_2; 7.2554) and q_e value (5.92 mg/g) was determined from the slope and intercept of the plot, Fig. 11b. The values of the correlation coefficients (R^2; 0.9949) was found almost equal to one. Accordingly, the kinetics of MB adsorption can be described well by the second-order equation in agreement with other published results [59,60]. That suggests that the rate-limiting step in

Table 3
R^2 values for the MB removal with the different studied equilibrium isotherms

Isotherm model	Parameters		
Langmuir	K_L (L/g)	q_{max} (mg/g)	R^2
	23.54	15.48	0.9693
Freundlich	K_F (mg/g)	N	R^2
	1.042	0.4910	0.9842
Harkin-Jura	B_H (mg^2/L)	A_H (g^2/L)	R^2
	1.663	4.655	0.8227
Temkin	K_T (L/g)	b_t (J/mol)	R^2
	0.866	10.216	0.8776

these sorption processes may be chemisorption involving valent forces through the sharing or exchange of electrons between adsorbent and adsorbate [61].

3.4.3. Elovich model

From the slope and intercept of the linearization of the simple Elovich equation, the estimated Elovich equation parameters were obtained (Fig. 11c). The value of β is indicative of the number of sites available for adsorption (1.361) while α value (2.1694) is the adsorption quantity when Ln t is equal to zero; that is, the adsorption quantity when t is 1 h. This value helps understand the adsorption behaviour of the first step [62]. Also, from this figure, it was declared that the Elovich equation fits well with the experimental data.

3.5. Adsorption mechanism models

Following up the adsorption mechanism of any ions onto solid from aqueous phase is going through a multi-step process. Initially, two steps were recognized in the liquid phase. The first step is the transport of the ions from the aqueous phase to the surface of the solid particles, which is known as bulk diffusion. This step was followed by diffusion of the ions via the boundary layer to the surface of the solid particles (film diffusion). The last step, consequently, happened in the solid phase where the ions transport from the solid particles surfaces to its interior pores, known as pore diffusion or intraparticle diffusion. This step is likely to be slow, and therefore, it may be considered as the rate-determining step.

Adsorption of an ion at an active site on the solid phase surface could also occur through a chemical reaction such as ion-exchange, complexation and chelation.

The diffusion rate equations inside particulate of Dumwald–Wagner and intraparticle models were used to calculate the diffusion rate of MB on ZnO nanoparticles. On the other hand, concerning the external mass transfer, Boyd model was examined to determine the actual rate-controlling step for MB removal.

Usually, the adsorption process was controlled by either the intraparticle (pore diffusion) or the liquid-phase mass transport rates (film diffusion) [63]. Experimenting is
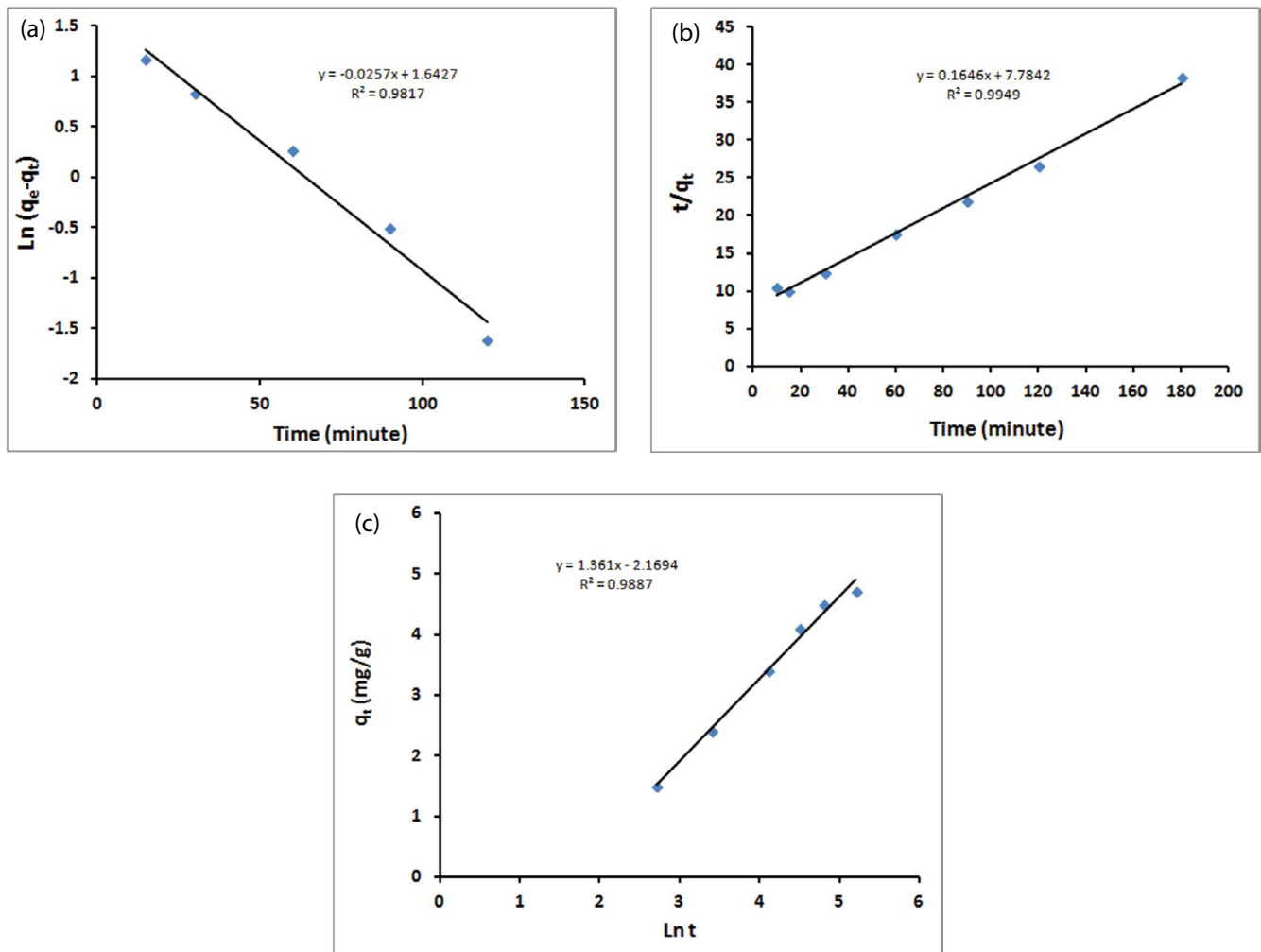
Fig. 11. Adsorption kinetic models: (a) pseudo-first-order model, (b) pseudo-second-order model and (c) Elovich model.

a batch system with rapid stirring lefts the possibility that intraparticle diffusion is the rate-determining step [64]. Weber and Morris explored the possibility of affecting the adsorption process via intra-particle diffusion resistance [65] using the intra-particle diffusion model described as follows:

$$q_t = k_{id}\, t^{\frac{1}{2}} + I \tag{11}$$

where k_{id} is the intra-particle diffusion rate constant. Weber and Morris [65] have figured out the thickness of the boundary layer from the values of I. Greater boundary layer effect was noticed with more significant intercept [66]. The plot of q_t vs. $t^{0.5}$ is presented in Fig. 12a. Two separate linear portions that represent each line could be observed from the figure. These two linear portions in the intraparticle model suggest that the removal process consists of both surface removal and intraparticle diffusion. While the initial linear part of the plot is the indicator of the existence of the boundary layer effect, the second linear portion is due to intraparticle diffusion [67]. The intraparticle diffusion rate (k_d), 0.081

(mg/g min), was calculated from the slope of the second linear portion and the values of C (3.6134), the intercept, provides an idea about the thickness of the boundary layer. The larger the intercept, the greater is the boundary layer effect [66].

In case of involving the intraparticle diffusion in the sorption process, then a linear relationship would result from the plot of q_t vs. $t^{1/2}$, and the intraparticle diffusion would be the controlling step if this line passed through the origin [63]. Fig. 12a confirms that straight lines were not passed through the origin. The difference between the rate of mass transfer in the initial and final steps of the sorption process may cause the deviation of straight lines from the origin. Accordingly, it can conclude that the pore diffusion is not the sole rate-controlling step [68]. Additional processes, such as the adsorption on the boundary layer, may also be involved in the control of the adsorption rate.

The diffusion rate equation inside particulate of Dumwald–Wagner can be expressed as [69]:

$$\log\left(1 - F^2\right) = -\left(\frac{K}{2.303}\right) \times t \tag{12}$$
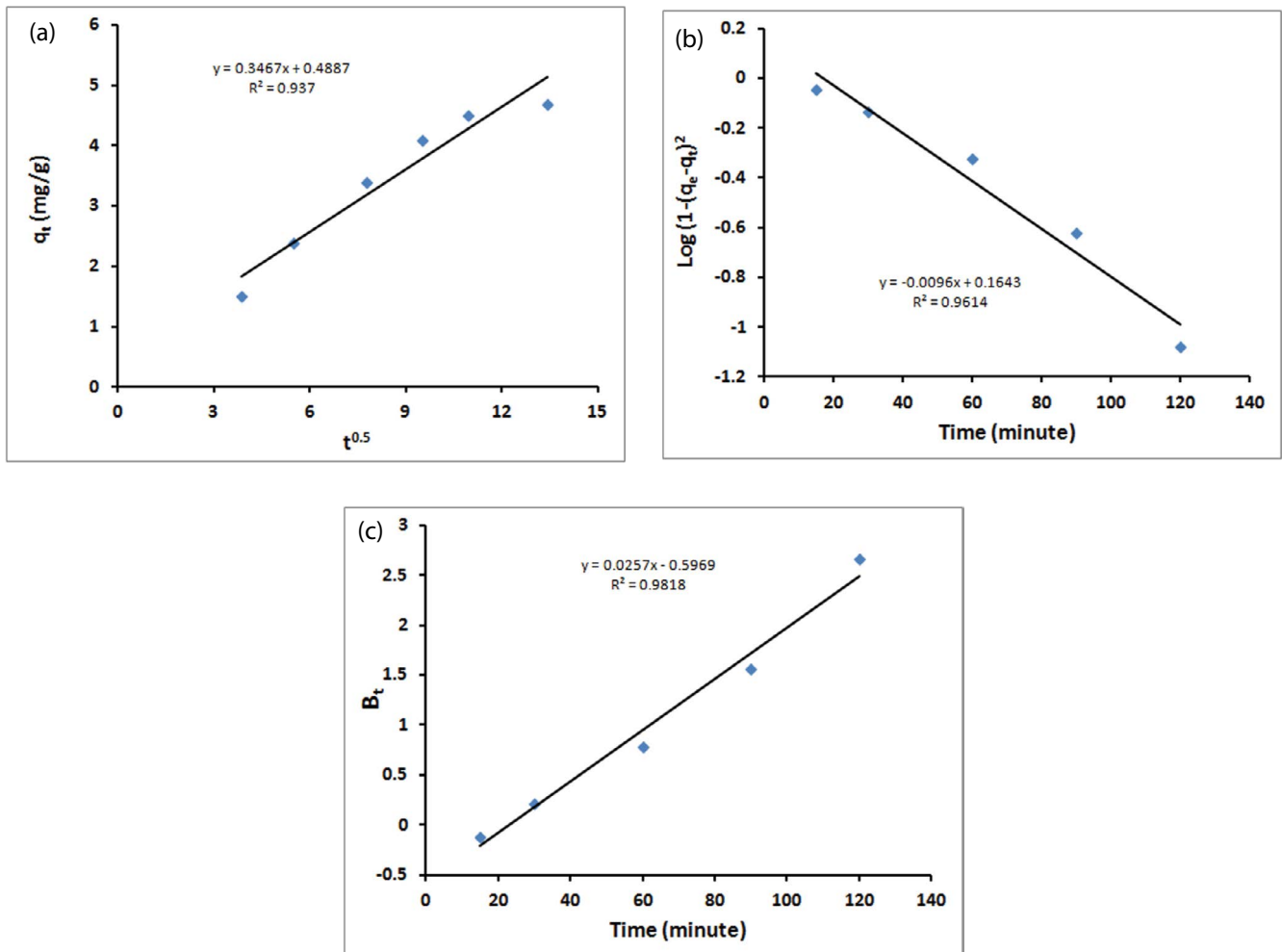
Fig. 12. Adsorption mechanism models: (a) intraparticle model, (b) Dumwald–Wagner and (c) Boyd model.

where K is the diffusion rate constant and the removal percentage, F is calculated by (q_t/q_e). The proper linear plot of log $(1-F^2)$ vs. t (Fig. 12b) indicates the applicability of this kinetic model. The diffusion rate constant K for MB diffusion inside ZnO nanoparticles was found −0.0221 min⁻¹.

The kinetic expression further analyzed the adsorption data is given by Boyd et al. [70] to characterize what the actual rate-controlling step involved in the MB sorption process.

$$F = 1 - \left(\frac{6}{\pi^2}\right) \exp\left(-B_t\right) \tag{13}$$

where F is the fraction of solute sorbed at different time t and B_t is a mathematical function of F and given by the following equation:

$$F = \frac{q}{q_\alpha} \tag{14}$$

q and q_α represent the amount adsorbed (mg/g) at any time t and at the infinite time (in the present study 7 h). With substituting Eq. (13) into Eq. (14), the kinetic expression becomes:

$$B_t = -0.4978 - \ln\left(\frac{1-q}{q_\alpha}\right) \tag{15}$$

Thus, the value of B_t can calculate for each value of "F" using Eq. (15). The calculated B_t values were plotted against time, as shown in Fig. 12c. The linearity of this plot will provide useful information to distinguish between external transport– and intraparticle transport–controlled rates of sorption. Fig. 11c shows the plot of B_t vs. t, which is a straight line that does not pass through the origin, indicating that the film diffusion governs the rate-limiting process [71].

3.6. Adsorption thermodynamic studies

The effect of variation adsorption temperature is illustrated previously in Fig. 5. A positive impact of elevating the adsorption temperature of MB has been observed. Such finding is an indication of the endothermic nature of the MB adsorption process on ZnO nanoparticles adsorbent.

From engineering aspects, the values of thermodynamic parameters such as the enthalpy change ($\Delta H°$), the free energy change ($\Delta G°$), and the entropy change ($\Delta S°$) should

be taken into consideration to conclude the spontaneity of the adsorption process. A spontaneous system will display a decrease in $\Delta G°$ and $\Delta H°$ values with increasing the temperature. All the thermodynamic parameters were calculated from the following equations [72,73]:

$$\ln K_0 = \frac{\Delta S}{R} - \frac{\Delta H}{RT} \qquad (16)$$

where:

$$K_0 = \frac{q_e}{C_e} \qquad (17)$$

$$\Delta G = -RT \ln K_0 \qquad (18)$$

where R is the gas constant (8.314 J/mol K), and T is the temperature in K. Table 4 lists down the values for the thermodynamic parameters (Fig. 13). The positive value for the $\Delta H°$ (27.78 kJ/mol) indicates the endothermic nature of the process, which explains the increase of MB adsorption efficiency as the temperature increased. As informed by Alkan et al. [74], the enthalpy change values as a result of the chemisorption are between 40 and 120 kJ mol^{-1}, which are more significant than that caused by the physisorption. Consequently, the lower value of the heat of adsorption acquired in this study indicates that the adsorption of MB is probably attributable to the physisorption. Conversely, in the kinetics study, it was described that the adsorption is chemisorption. Thus, it is evident from the lower $\Delta H°$ value that the physisorption also takes part in the adsorption process in which the MB ions adhere to the adsorbent surface only through weak intermolecular interactions. The positive value for the entropy change, $\Delta S°$ (83.47 J/mol K) illustrating the disorderliness at the solid/liquid interface during the adsorption of MB ions onto the ZnO nanoparticles. The $\Delta G°$ values reflect the feasibility of the process.

3.7. Effect of the ZnO nanoparticles size

The effect of ZnO nanoparticles size variation on the adsorption capacity has been explored. From Fig. 14 it is clear that the particles size has a direct impact on the adsorption capacity of the ZnO nanoparticles. An inversely proportional relation has been realized from the figure where the increment of the adsorption capacity of the ZnO nanoparticles

is accompanied with a decrease of the particles size. This relation is a linear one in the particles size between 194 nm and 139 nm, then turned to be exponential one with particle size below 100 nm where the capacity increase from 4.4 to 6.738 mg/g for 139 nm and 98.5 nm particles. This behaviour is closely related to the increase of the contacted surface area of the ZnO nanoparticles with the MB solution, which reflects on the affinity to adsorb the MB molecules. The affinity has been measured by the distribution coefficient (K_d) which correlate the amount of the adsorbed MB onto ZnO nanoparticles (solid phase) to its concentration in the solution (liquid phase) at equilibrium according to the following relation:

$$K_d = \frac{q_e}{C_e} \qquad (19)$$

The detected behaviour of the K_d is quite similar to the adsorption capacity. Also, the value of the K_d for ZnO particle size below 100 nm (1.0328 Lg^{-1}) is much higher than the counterpart particle size over 100 nm to 193 nm which
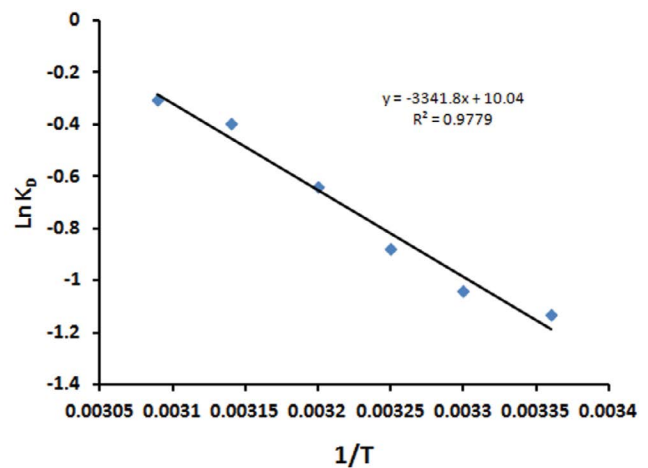
Fig. 13. Van't Hoff plot of the adsorption of MB onto ZnO nanoparticles.
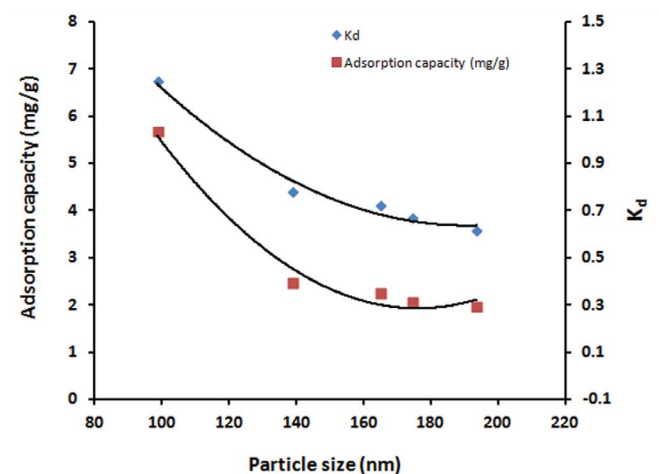
Fig. 14. Effect of the particles size on the adsorption capacity and the distribution coefficient (K_d).

Table 4
Thermodynamic parameters

Temperature (°C)	Thermodynamic parameters		
	ΔG (kJ mol^{-1})	ΔH (kJ mol^{-1})	ΔS (J K^{-1} mol^{-1})
25	2.8046	27.78	83.47
30	2.62		
35	2.2421		
40	1.6673		
45	1.0472		
50	0.8249		

fall in the range 0.3 to 0.4 Lg⁻¹. The adsorbent was classified according to the K_d value as a good one with a value between 1.0 and 10.0 Lg⁻¹ and as outstanding adsorbent with K_d value over 10.0 Lg⁻¹. Accordingly, the ZnO nanoparticles size less than 100 nm considered as a good adsorbent.

4. Conclusion

Highly chelating alginate derivatives (phosphorylated alginate; PhAlg) were developed and used as a template for preparation of zinc oxide (ZnO) nanoparticles with varied size. The structure and morphology of the obtained ZnO nanoparticles were verified using FT-IR, SEM, TGA, and surface area characterization tools.

The prepared zinc oxide nanoparticles were tested for the removal of the methylene blue (MB) from its aqueous solutions in batch experiments under different operational conditions. It was found that the initial MB concentration, the adsorbent dosage and the adsorption temperature have a positive impact on the adsorption capacity of the ZnO nanoparticles adsorbent. While 180 min of adsorption time was found enough to establish equilibrium and pH 7.0 is optimum for maximum adsorption capacity.

Fitting the results with different kinetic models shows that the adsorption process was followed by the pseudo-second-order model. The MB adsorbed as monolayers over the ZnO nanoparticles surface as proven by Langmuir isotherm model. The maximum adsorption capacity, according to Langmuir, was found to be 15.48 mg/g. The application of different diffusion models indicated that film diffusion governs the rate-limiting process. Moreover, the thermodynamics of the adsorption process proved the endothermic nature of the adsorption process.

Finally, the particles size was found to be a determined factor where the size below 100 nm was found useful according to the adsorption capacity and the distribution coefficient values.

In conclusion, the ZnO nanoparticles with size below 100 nm are suitable adsorbents for the removal of cationic contaminants from wastewater. Further investigations to control the ZnO particles size are needed.

References

[1] E. Taylor, T.J. Webster, Reducing infections through nanotechnology and nanoparticles, Int. J. Nanomed., 6 (2011) 1463–1473.

[2] P. Asharani, Y.L. Wu, Z. Gong, S. Valiyaveettil, Toxicity of silver nanoparticles in zebrafish models, Nanotechnology, 19 (2008) 255102.

[3] M.S. Tokumoto, V. Briois, C.V. Santilli, Preparation of ZnO nanoparticles: structural study of the molecular precursor, J. Sol-Gel Sci. Technol., 26 (2003) 547–551.

[4] H. Oh, J. Krantz, I. Litzov, T. Stubhan, L. Pinna, C. Brabec, Comparison of various sol gel derived metal oxide layers for inverted organic solar cells, Sol Energy Mater. Sol C, 95 (2011) 2194–2199.

[5] X.Y. Zhao, B.C. Zheng, C.Z. Li, H.C. Gu, Acetate-derived ZnO ultrafine particles synthesized by spray pyrolysis, Powder Technol., 100 (1998) 20–23.

[6] T. Tani, L. Mädler, S.E. Pratsinis, Homogeneous ZnO nanoparticles by flame spray pyrolysis, J. Nanoparticles Res., 4 (2002) 337–343.

[7] X. Li, G. He, G. Xiao, H. Liu, M. Wang, Synthesis and morphology control of ZnO nanostructures in microemulsions, J. Colloid Interface Sci., 333 (2009) 465–473.

[8] Z.R. Dai, Z.W. Pan, Z.L. Wang, novel nanostructures of functional oxides synthesized by thermal evaporation, Adv. Funct. Mater., 13 (2003) 9–24.

[9] I. Amarilio-Burshtein, S. Tamir, Y. Lifshitz, Growth modes of ZnO nanostructures from laser ablation, Appl. Phys. Lett., 96 (2010) 104–106.

[10] W.I. Park, C.H. Lee, J.H. Chae, D.H. Lee, G.C. Yi, Ultrafine ZnO nanowire electronic device arrays fabricated by selective metal-organic chemical vapor deposition, Small, 5 (2009) 181–184.

[11] L.C. Damonte, L.A. Mendoza Zélis, B. MaríSoucase, M.A. Fenollosa, Nanoparticles of ZnO obtained by mechanical milling, Powder Technol., 148 (2004) 15–19.

[12] S. Komarneni, M. Bruno, E. Mariani, Synthesis of ZnO with and without microwaves, Mater. Res. Bull., 35 (2000) 1843–1847.

[13] M. Bitenc, P. Podbršček, C.Z. Orel, M.A. Clevel, J.A. Paramo, R.M. Peters, Correlation between morphology and defect luminescence in precipitated zno nanorod powders, Cryst. Growth Des., 9 (2009) 997–1001.

[14] O. Carp, D. Visinescu, G. Patrinoiu, A. Tirsoaga, Green synthetic strategies of oxide materials: polysaccharides-assisted synthesis. Part IV. Alginate-assisted synthesis of nanosized metal oxides, Rev. Roum. Chim., 56 (2011) 901–906.

[15] S. Plumejeau, J.G. Aalauzun, B. Boury, Hybrid metal oxide@ biopolymer materials precursors of metal oxides and metal oxide-carbon composites, Ceramic Soc. Japan, 123 (2015) 695–708.

[16] A. Arora, V.S. Jaswalk, K. Singh, R. Singh, Metal/metal oxides and their applications as adsorbents, Int. J. Chem. Sci., 14 (2016) 3215–3227.

[17] R.F. Mulligan, A.A. Iliadis, P. Kofinas, Synthesis and characterization of ZnO nanostructures templated using diblock copolymers, J. Appl. Polym. Sci., 89 (2003) 1058–1061.

[18] Z. Schnepp, S.C. Wimbush, S. Manna, S.R. Hall, Alginate-mediated routes to the selective synthesis of complex metal oxide nanostructures, Cryst. Eng. Comm., 12 (2010) 1410–1415.

[19] M. Thirumavalavan, K.-.L Huang, J.-F. Lee, Preparation and morphology studies of nano zinc oxide obtained using native and modified chitosans, Materials, 6 (2013) 4198–4212.

[20] D. Ramimoghadam, M.Z.B. Hussein, Y.H. Taufiq-Yap, Hydrothermal synthesis of zinc oxide nanoparticles using rice as soft biotemplate, Chem. Cent. J., 7 (2013) 136–145.

[21] S. Mandal, D. Savio, S.J. Selvaraj, S. Natarajan, A.B. Mandal, Micro-structural properties of zinc oxide nano-particles synthesized by bio-polymeric templates, Adv. Mater. Res., 906 (2014) 190–195.

[22] P. Vasileva, Synthesis and characterization of ZnO nanocrystals in starch matrix, Scientific Proc. II International Scientific Conference "Material Science. Non-Equilibrium Phase Transformations", Vol. XXIV, 2016, pp. 33–36.

[23] S.A. Shewala, V.A. Kalantre, G.S. Gokavi, Hydrothermal synthesis of ZnO nanospheres with sodium alginate as template and its photocatalytic application for degradation of diclofenac and chloroamphenicol, Indian J. Chem., 56A (2017) 949–954.

[24] T. Robinson, G. McMullan, R. Marchant, P. Nigam, Remediation of dyes in textile effluent: a critical review on current treatment technologies with a proposed alternative, Bioresour. Technol., 77 (2001) 247–262.

[25] Y.Z. Chen, N. Li, Y. Zhang, L.D. Zhang, Novel low-cost Fenton-like layered Fe-titanate catalyst: preparation, characterization and application for degradation of organic colorants, J. Colloid Interface, 422 (2014) 9–15.

[26] M. Shah, Effective treatment systems for azo dye degradation: a joint venture between physico-chemical and microbiological process, Int. J. Environ. Bioremed. Biodegrad., 2 (2014) 231–242.

[27] E. Forgas, T. Cserhati, G. Oras, Removal of synthetic dyes from wastewater: a review, Environ. Int., 30 (2004) 953–971.

[28] H. Nourmoradi, A.R. Ghiasvand, Z. Noorimotlagh, Removal of methylene blue and acid orange 7 from aqueous solutions by activated carbon coated with zinc oxide (ZnO) nanoparticles: equilibrium, kinetic, and thermodynamic study, Desal. Wat. Treat., 55 (2015) 252–262.

[29] H.A. Sani, H.S. Aliyu, S.A. Tukur, Methylene blue dye adsorption using a polymer coated ZnO with chitosan nano-catalyst, IOSR J. Appl. Chem., 8 (2015) 34–38.

[30] N. Prabha, M. Vennila, Equilibrium and kinetic studies on adsorption of methylene blue dye by ZnO nanoparticles synthesized by hydrothermal method, J. Appl. Sci. Eng. Meth., 2 (2016) 388–393.

[31] I.K. Al-Khateeb, M.S. Mahmood, Adsorption, Thermodynamics and kinetics of methylene blue on nano structured ZnO crystals, Am. Chem. Sci. J., 13 (2016) 1–9.

[32] A.V. Kulkarni, A. Chavhan, A. Bappakhane, J. Chimmankar, ZnO nanoparticles as adsorbent for removal of methylene blue dye, Res. J. Chem. Environ. Sci., 4 (2016) 158–163.

[33] W.M. Abou-Taleb, G.D. Roston, M. S Mohyeldin, A. M Omer, T.M. Tamer, E.F. Shehata, A.M. Hafez, Functionalization of alginate via phosphorization: preparation, and characterization, Int. J. Adv. Res., 5 (2017) 1612–1621.

[34] T.M. Tamer, W.M. Abou-Taleb, G.D. Roston, M.S. Mohyeldin, A.M. Omer, E.F. Shehata, Characterization and evaluation of iron oxide nanoparticles prepared using hydrogel template based on phosphonate alginate, Nanosci. Nanotechnol-Asia, 7 (2017) 220–232.

[35] T.M. Tamer, W.M. Abou-Taleb, G.D. Roston, M.S. Mohyeldin, A.M. Omer, R.E. Khalifa, A.M. Hafez, Formation of zinc oxide nanoparticles using alginate as a template for purification of wastewater, Environ. Nanotechnol, Monit. Manage., 10 (2018) 112–121.

[36] A.K. Mishra, D. Das, Investigation on Fe-doped ZnO nanostructures prepared by a chemical route, Mater. Sci. Eng. B Adv., 171 (2010) 5–10.

[37] K.S. Fernandes, E. de Azevedo Alvarenga, P.R.G. Brando, V. de Freitas Cunha Lins, Infrared-spectroscopy analysis of zinc phosphate and nickel and manganese modified zinc phosphate coatings on electrogalvanized steel, Rem. Revista. Escola de Minas, 64 (2011) 45–49.

[38] R. Wahab, S.G. Ansari, Y.S. Kim, H.K. Seo, G.S. Kim, G. Khang, H.-S. Shin, Low temperature solution synthesis and characterization of ZnO nano-flowers, Mater. Res. Bull., 42 (2007) 1640–1648.

[39] H. Liu, D. Yang, H. Sun, Z. Zhu, Microwave - assisted hydrothermal synthesis and characterization of hierarchical structured ZnO nanorods, J. Optoelectron. Adv. Mater., 12 (2010) 2063–2068.

[40] T. Thangeeswari, A.T. George, A.A. Kumar, Optical properties and FTIR studies of cobalt doped ZnO nanoparticles by simple solution method, Indian J. Sci. Technol., 9 (2016) DOI: 10.17485/ijst/2016/v9i1/85776.

[41] X.S. Wang, Y. Zhou, Y. Jiang, C. Sun, The removal of basic dyes from aqueous solutions using agricultural by-products, J. Hazard. Mater., 157 (2008) 374–385.

[42] V. Belessi, G. Romanos, N. Boukos, D. Lambropoulou, C. Trapalis, Removal of Reactive Red 195 from aqueous solutions by adsorption on the surface of TiO_2 nanoparticles, J. Hazard. Mater., 170 (2009) 836–844.

[43] M. Wawrzkiewicz, Removal of C.I. Basic Blue 3 dye by sorption onto cation exchange resin, functionalized and non-functionalized polymeric sorbents from aqueous solutions and wastewaters, Chem. Eng. J., 217 (2013) 414– 425.

[44] Y.F. Shen, J. Tang, Z.H. Nie, Y.D. Wang, Y. Ren, L. Zuo, Preparation and application of magnetic Fe_3O_4 nanoparticles for wastewater purification, Sep. Purif. Technol., 68 (2009) 312–319.

[45] K. A. Al-Saad, M. A. Amr, D.T. Hadi, R. S. Arar, M. M. AL-Sulaiti, T. A. Abdulmalik, N. M. Alsahamary, J. C. Kwak, Iron oxide nanoparticles: applicability for heavy metal removal from contaminated water, Arab. J. Nucl. Sci. Appl., 45 (2012) 335–346.

[46] F. Rozada, L.F. Calvo, A.I. Garcia, J. Martin-Villacorta, M. Otero, Dye adsorption by sewage sludge-based activated carbons in batch and fixed-bed systems, Bioresour. Technol., 87 (2003) 221–230.

[47] G. Gode, E. Pehlivan, Adsorption of Cr(III) ions by Turkish brown coals, Fuel Process Technol., 86 (2005) 875–884.

[48] Y.S. Ho, Effect of pH on lead removal from water using tree fern as the sorbent, Bioresour. Technol., 96 (2005) 1292–1296.

[49] N. Unlü, M. Ersoz, Adsorption characteristics of heavy metal ions onto a low cost biopolymeric sorbent from aqueous solutions, J. Hazard. Mater., 136 (2006) 272–280.

[50] A. Mohammad, A.K.R. Rifaqat, A. Rais, A. Jameel, Adsorption studies on citus reticulate (fruit peel of orange): removal and

[51] A. Stolz, Basic and applied aspects in the microbial degradation of azo dyes, Appl. Microbiol. Biotechnol., 56 (2001) 69–80.

[52] B.H. Hameed, L.H. Chin, S. Rengaraj, Adsorption of 4-chlorophenol onto activated carbon prepared from rattan sawdust, Desalination, 225 (2008) 185–198.

[53] M.I. Temkin, V. Pyzhev, Kinetics of ammonia synthesis on promoted iron catalyst, Acta Physiochim. URSS, 12 (1940) 327–356.

[54] I.A.W. Tan, A.L. Ahmad, B.H. Hameed, Adsorption isotherms, kinetics, thermodynamics and desorption studies of 2,4,6-trichlorophenol on oil palm empty fruit bunch-based activated carbon, J. Hazard. Mater., 164 (2009) 473–482.

[55] M.J. Tempkin, V. Pyozhev, Kinetics of ammonia synthesis on promoted iron catalyst, Acta Physicochim URSS, 12 (1940) 327–352.

[56] A.U. Itodo, H.U. Itodo, Sorption energies estimation using Dubinin-Radushkevich and Temkin adsorption isotherms, Life Sci. J., 7 (2010) 31–39.

[57] M.M. Dubinin, E.D. Zaverina, L.V. Radushkevich, Sorption and structure of active carbons I. adsorption of organic vapors, Zhurnal Fizicheskoi Khimii, 21 (1947) 1351–1362.

[58] M. Ozacar, I.A. Sengil, A kinetic study of metal complex dye sorption onto pinedust, Process Biochem., 40 (2005) 565–572.

[59] G. Kiani, M. Khodagholizadeh, M. Soltanzadeh, Removal of methylene blue by modified polyacrylonitrile from aqueous solution, CTAIJ, 8 (2013) 121–127.

[60] M.A. Abu-Saied, E.S. Abdel-Halim, Moustafa M.G. Fouda, Salem S. Al-Deyab, Preparation and characterization of iminated polyacrylonitrile for the removal of methylene blue from aqueous solutions, Int. J. Electrochem. Sci., 8 (2013) 5121–5135.

[61] Y.S. Ho, G. McKay, Pseudo-second order model for sorption processes, Process Biochem., 34 (1999) 451–465.

[62] R.L. Tseng, Mesopore control of high surface area NaOH-activated carbon, J. Colloid Interface Sci., 303 (2006) 494–502.

[63] G. Crini, H.N. Peindy, F. Gimbert, C. Robert, Removal of C. I. Basic Green 4 (Malachite Green) from aqueous solutions by adsorption using cyclodextrin-based adsorbent: kinetic and equilibrium studies, Sep. Purif. Technol., 53 (2007) 97–110.

[64] G. McKay, The adsorption of dyestuffs from aqueous solution using activated carbon: analytical solution for batch adsorption based on external mass transfer and pore diffusion, Chem. Eng. J., 27 (1983) 187–195.

[65] W.J. Weber, J.C. Morris, Kinetics of adsorption on carbon from solution, J. Sanit. Eng. Div. Am. Soc. Civil Eng., 89 (1963) 31–59.

[66] K. Kannan, M.M. Sundaram, Kinetics and mechanism of removal of methylene blue by adsorption on various carbons—a comparative study, Dyes Pigm., 51 (2001) 25–40.

[67] M. Sarkar, P.K. Acharya, B. Bhaskar, Modeling the removal kinetics of some priority organic pollutants in water from diffusion and activation energy parameters, J. Colloid Interface Sci., 266 (2003) 28–32.

[68] V.J.P. Poots, G. McKay, J.J. Healy, Removal of basic dye from effluent using wood as an adsorbent, J. Water Pollut. Cont. Fed., 50 (1978) 926–939.

[69] G. McKay, M.S. Otterburn, J.A. Aja, Fuller's earth and fired clay as adsorbents for dye stuffs, Water Air Soil Pollut., 24 (1985) 307–322.

[70] G.E. Boyd, A.W. Adamson, I.S. Myers, The exchange removal of ions from aqueous solutions by organic zeolites; kinetics, J. Am. Chem. Soc., 69 (1947) 2836–2848.

[71] A.E. Ofomaja, Kinetic study and sorption mechanism of methylene blue and methyl violet onto mansonia (*Mansonia altissima*) wood sawdust, Chem. Eng. J., 143 (2008) 85–95.

[72] T.A. Khan, S. Dahiya, I. Ali, Use of kaolinite as adsorbent: equilibrium, dynamics and thermodynamic studies on the adsorption of Rhodamine B from aqueous solution, Appl. Clay Sci., 69 (2012) 58–66.

[73] G. Zhao, J. Li, X. Wang, Kinetic and thermodynamic study of 1-naphthol adsorption from aqueous solution to sulfonated graphene nanosheets. Chem. Eng. J., 173 (2011) 185–190.

[74] M. Alkan, O. Demirbas, S.Ç.M. Dogan, Sorption of acid red 57 from aqueous solution onto sepiolite, J. Hazard. Mater., B116 (2004) 135–145.